



# Modeling of Deposition Geometry in Laser Directed Energy Deposition over Inclined Surfaces for Restoration and Remanufacturing

Sachin Alya<sup>1</sup> · Chaitanya Vundru<sup>1,2</sup> · Bhargavi Ankamreddy<sup>1</sup> · Ramesh Singh<sup>1</sup>

Received: 7 March 2021 / Accepted: 22 June 2021 / Published online: 2 July 2021  
© Indian National Academy of Engineering 2021

## Abstract

Additive manufacturing has gained much popularity in the last decade because of its flexibility and sustainability. One of the leading additive manufacturing processes is laser-directed energy deposition (LDED). In addition to building three-dimensional free-form features, LDED has a huge potential in the repair and reconditioning segment of the industry. A variety of valuable components such as dies, molds, turbine blades, valves, etc. subjected to high thermal and mechanical loads develop surface defects over time. These components can be restored to their functional condition using LDED instead of replacing them. The material similar to substrate material or even better can be deposited using LDED. These components generally possess complex free-form features and contours, which makes it difficult to perform depositions keeping the deposition head vertical and requires the deposition head to be inclined to the desired inclination angle, which may affect the powder catchment and the deposition geometry. The effect of the inclination angle on the catchment and the deposition geometry needs to be studied for a better understanding of the DED process. In this paper, the different strategies of deposition over inclined surfaces have been studied. Based on the experimental results, a phenomenological model is developed to predict the powder catchment efficiencies at depositions with different inclinations. The inclination not only affects the effective powder reaching the melt pool but also affects the shape of the deposition. A two-dimensional computational fluid dynamics (CFD) model has also been developed, which predicts the shape of the deposition cross-section. The model considers the flow of the melt pool, due to inclination, before solidification. The model captures the effect of inclination angle in terms of reduction in powder catchment efficiency (PCE) and the gravity-driven melt flow effectively.

**Keywords** Laser directed energy deposition (LDED) · Additive manufacturing · Deposition geometry

## Introduction

Sustainability is a watchword for the current world scenario, and a key to that is restoration. The mechanical and structural components, heavy machinery, and equipment employed in forging, injection molding, power plants, aerospace industries, etc., are subjected to cyclic thermomechanical loading. The cyclic thermomechanical loads can induce localized wear and damage in the components making them unusable, which may mandate a product replacement.

Product replacement is costly and time-intensive, which can be avoided if the components are restored instead. There are numerous methods with which a damaged component can be restored, like arc welding and thermal spraying. These processes do not possess adequate controllability and precision, which may thermally damage and distort the component. Accurate repair requires a precise and focused heating source and, hence, laser-based processes having high controllability can be used effectively for the repair of such worn/damaged components.

For hard-facing, additive manufacturing, and 3D free form repair, laser directed energy deposition (LDED) is a promising technique. This technique is suitable for the repair of high-value components, like turbine blades, molds, and dies, valve seats, and boiler components (Jhavar et al. 2013). LDED uses a laser beam as a heat source for controlled heating that melts a thin layer of the substrate along with the powder, which fuses to form a sound metallurgical bond.

✉ Ramesh Singh  
rsingh@iitb.ac.in

<sup>1</sup> Department of Mechanical Engineering, Indian Institute of Technology Bombay, Mumbai 400076, Maharashtra, India

<sup>2</sup> Department of Mechanical and Aerospace Engineering, Monash University, Clayton, Melbourne VIC 3800, Australia

Hot-work steels are the most popular material used for the manufacture of tooling in forming and molding industries. Among the chromium-molybdenum hot work steels, H13 has an excellent combination of toughness and resistance to thermal fatigue, which makes it very attractive. Crucible powder metallurgical (CPM) steels with high Vanadium contents can be used for repairing such components because CPM steels possess an exceptional combination of properties, like toughness, hardness, and wear resistance (Kattire et al. 2015; Paul et al. 2017). Repairing the components with CPM steels can not only restore them to their operational condition but in some cases, even enhance the functional performance. A study (Leunda et al. 2011) reported a repair application performed using a coating of CPM 10 V. Subsequently, deposition of consolidated 3D structures of CPM 9 V and H13 was reported by (Xue et al. 2013). It was observed that the deposited structures had unique, refined microstructures and excellent mechanical properties. CPM 10 V and CPM 15 V were used for hard facing of cutting and stamping dies made of AISI 1045 (Hu et al. 1998). Apart from these, the study for the evaluation of resistance to abrasion of coatings of CPM 9 V, 10 V, and 15 V was done (Wang et al. 2006). Thermomechanical and fully coupled metallurgical and thermomechanical models of the repair process for predicting residual stresses and dilution using CPM 9 V steel have been reported in the literature (Vundru et al. 2019, 2020a, b).

It can be noted that for the repair of components using DED, it is of utmost importance to consider the geometrical complexity of the components. Most of the components have contoured surfaces which necessitates deposition of material at various angles of inclination. Therefore, it becomes imperative to evaluate the characteristics of LDED over inclined surfaces. Very limited work has been reported in the literature on the effect of angle of inclination of the substrate in LDED. Lin and Hwang (1999) studied the powder catchment in laser cladding over an inclined surface. In this study, the laser axis was always kept vertical, however, the substrate was inclined at an angle, which changes the mode shape of laser and powder on the surface of the substrate. In another study (Bruck et al. 2012), the effect of angle of incidence of the laser beam on the clad characteristics was investigated. The effect of gravity-driven melt flow and viscous force on the melt pool has been characterized (Alya et al. 2019, 2021). The characterization of the clad cross-section with substrate inclination has also been studied by Zhu et al. (2017). Their experimental setup used an annular laser beam, and the powder was fed within the beam at inclinations up to 150°. A study by Paul et al. (2013) reported a novel nozzle design for laser cladding over vertical surfaces. Besides, their work also presented analytical modeling and experimental characterization of clad shapes obtained with cladding over vertical surfaces. The influence of nozzle

inclination on the powder flow characteristics and effective powder catchment via a discrete phase model has also been studied (Alya and Singh 2021).

The depositions over inclined surfaces result in skewed deposition geometries due to the effect of the asymmetric gravity vector on the melt pool. To predict the clad shape, a computational fluid dynamics model can be employed. The fluid flow in the melt pool, heat transfer, and solidification is the critical physical phenomenon that governs the final clad shape. Various numerical models have been reported in the literature for the prediction of deposition geometry (Qi et al. 2006; Paul et al. 2016). An analytical model has been developed for the prediction of clad geometry for various nozzle-substrate tilt combinations (Hao et al. 2019). This model considers the surface tension and viscous effect but has not incorporated the solidification of the melt pool. Characterization of clad geometry in micro-scale laser deposition has been presented by Alya et al. (2017). L alas et al. (2007) evaluated the final clad shape by finding contact angles using the surface tension theory for symmetric clad on a flat surface. A finite element model employing sequential activation of elements to predict the clad shape was reported by Fallah et al. (2011).

To the best of the authors' knowledge, the dependence of the effective powder entrapment (powder catchment efficiency, PCE) and the subsequent gravity-driven melt-flow as a function of substrate inclination has not been reported in the literature. As the angle of inclination of the substrate increases, the effect of gravity on the flow dynamics of the powder jet in the nozzle becomes significant affecting the powder catchment efficiency. Besides powder loss at a higher angle of inclinations, the gravity-driven melt flow also affects the evolution of the deposition geometry. It is very important to understand and predict the shape evolution of deposited track in free-form repair. Hence, the effect of angle of inclination on the powder catchment efficiency has been investigated and presented in this paper. A CFD model has also been developed to incorporate the effect of gravity on the melt flow before solidification, and the shape of the deposition geometry has been predicted.

## Experimental Work

This section is focused on the experimental work and is comprised of the development of experimental setup and also provides complete parametric details used for performing experiments.

## Experimental Setup

The DED system has been developed in the Machine Tools Laboratory at the Indian Institute of Technology Bombay,

and all the experimental work presented in this study has been performed on this developed DED system. Generally, a DED system is composed of 5 subsystems: directed energy beam (laser), material deposition head, positioning system, material delivery system, and process gas supply.

The developed DED system comprises a 3 kW Ytterbium laser source (Make: IPG Photonics and Model: YLS-3000). The source emits a laser of wavelength  $1070 \pm 10$  nm. The laser source equipped in the DED system is customized for beam switching with dual-beam delivery fiber. The core diameters of the fibers are 100  $\mu\text{m}$  and 400  $\mu\text{m}$ . Either of the two can be employed based on the scale (micro or macro) of deposition required. The delivery ends of each fiber are fitted with QBH/HLC-8 connectors, which can be coupled with any standard material processing heads. In the developed system, the beam delivery fiber is coupled with a material deposition head (make: precitec and model: YC52). The optical components of the deposition head first collimate the beam and then focus it at a fixed point and yield 3X of magnification. This provides beam sizes from 300  $\mu\text{m}$  to few millimetres.

The powder feeding in the deposition head is performed using an annular coaxial nozzle which focuses and delivers the powder efficiently onto the substrate. A powder feeder (make: MEC and model: PF-3350) supplies the powder to the deposition head. For transportation of powder from powder feeder to deposition head, Argon is used as a carrier gas. The auxiliary gas used is also Argon which shields

the melt pool and protects the optical components as well by providing resistance to powder particles entering the laser path. The last requirement for the system is to have a desired movement and manoeuvrability, which can be achieved using a positioning system. In the present system, a robotic manipulator (make: KUKA and model: KR 20-3) is employed to attain free-form movement. The system is shown in Fig. 1.

All the functional requirements of a DED system can be fulfilled by the above-mentioned subsystems. However, manually operating and triggering these subsystems is difficult. With the aim to solve this problem, all the subsystems are integrated into the robotic manipulator via a programmable logic controller (PLC). This establishes communication between the robot controller and the integration panel, which further connects all the subsystems. With this, synchronized triggering of all the systems through the robot controller becomes possible. In addition to safeguarding the operator and containment of radiation, the whole system is enclosed inside an aluminium enclosure.

## Experimental Details

All the DED experiments were performed on the setup described in the previous section. The depositions were made with an angle of inclinations ranging from 0 to 75°, with an increment of 15°, to characterize the effect of angle of inclination on powder catchment efficiency and the

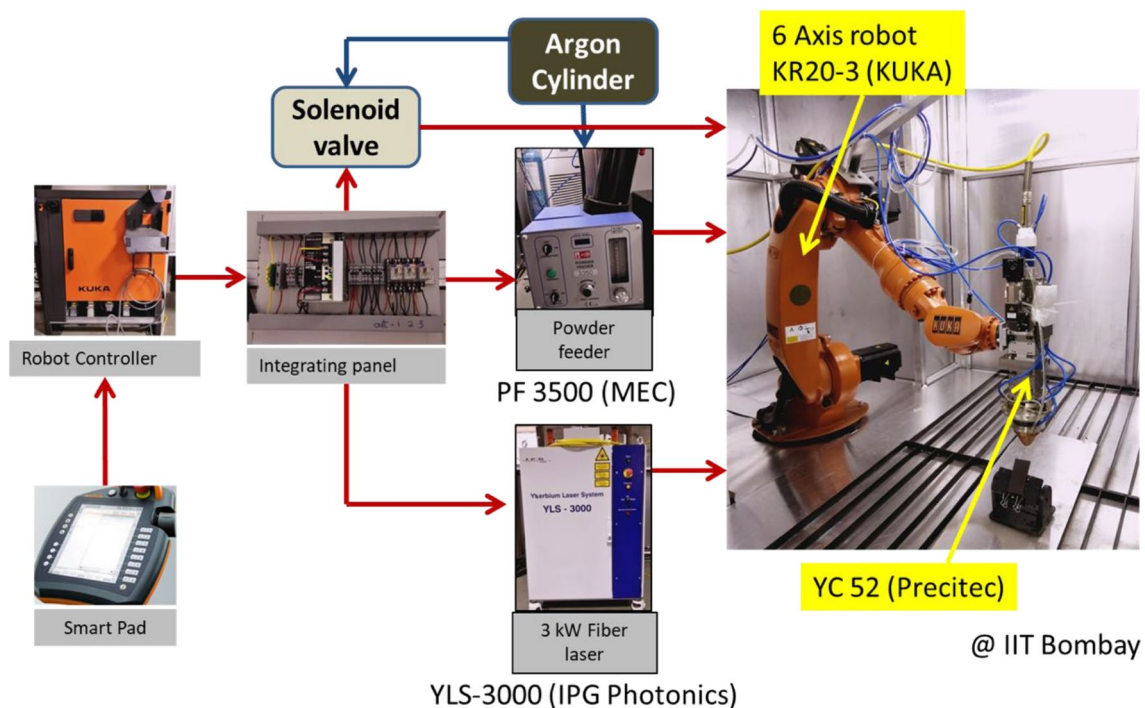


Fig. 1 Developed robotic DED system

deposition geometry. The other process parameters such as laser power, deposition speed, mass flow rate, and gas flow rate were kept constant. The details of fixed parameters are listed in Table 1.

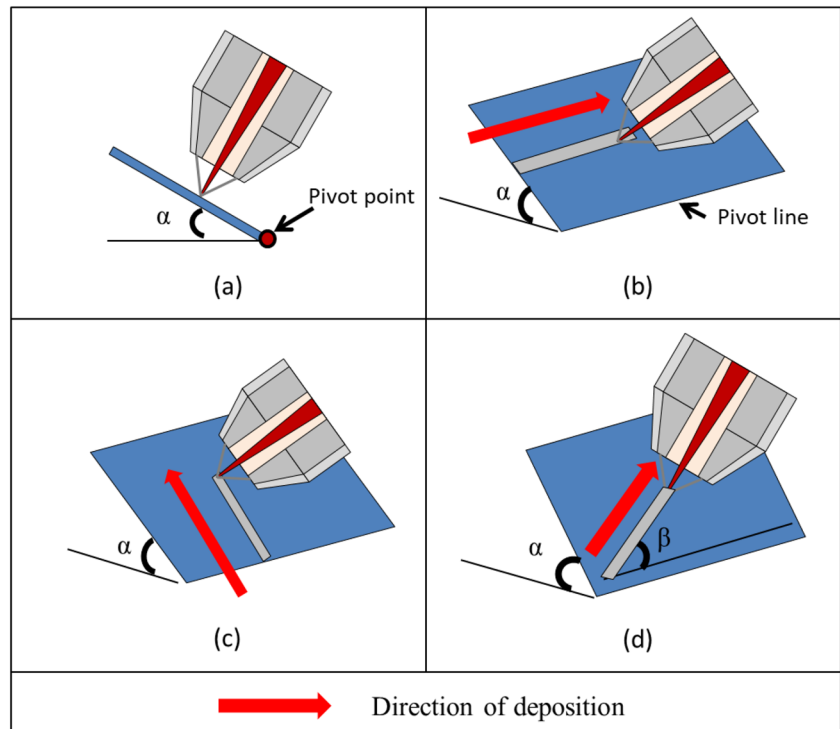
The depositions were carried out keeping the laser beam normal to the substrate surface. The schematic of the variation of deposition angles and directions of deposition is shown in Fig. 2. Figure 2b shows the pivot line about which the substrate is inclined. In this study, the following three strategies of deposition have been studied:

- Case 1: the depositions were carried out parallel to the pivot line and were called longitudinal deposition where only the angle  $\alpha$  was varied, as shown in Fig. 2b.
- Case 2: the depositions were carried out perpendicular to the pivot line and were called transverse deposition, where only the angle  $\alpha$  was varied, as shown in Fig. 2c.
- Case 3: in the third case, the depositions were carried out in an oblique direction, i.e., a combination of case 1 and case 2. The direction of deposition was a combination of angles  $\alpha$  and  $\beta$ , as shown in Fig. 2d.

**Table 1** Input parameter details

Parameter	Value	Units
Laser power	1800	W
Deposition speed	340	mm/min
Mass flow rate	26.9	g/min

**Fig. 2** DED process with inclination angle  $\alpha$  with (a) constant pivot point, (b) deposition parallel to the pivot line, (c) depositions carried out perpendicular to the pivot line, (d) depositions carried out in an oblique direction



In case 3, the inclination angle  $\alpha$  was kept constant at  $45^\circ$ , and the angle  $\beta$  was varied from  $15^\circ$  to  $75^\circ$ . The powder catchment efficiency (i.e., the percentage of powder supplied which was deposited over the surface) is characterized in this paper. The geometry of the deposition has also been evaluated for the aforementioned cases. Two repetitions were performed for each experimental condition.

The depositions were carried out using the powder particles of CPM 9 V (crucible particle metallurgy steel). The spherically atomized powder particle sizes varied between 75 and 210  $\mu\text{m}$ . The substrate used for deposition was H13 tool steel plates, and the gas used for powder carrying and the shielding was Argon (99.9995%). The chemical compositions of the powder and substrate materials are listed in Table 2.

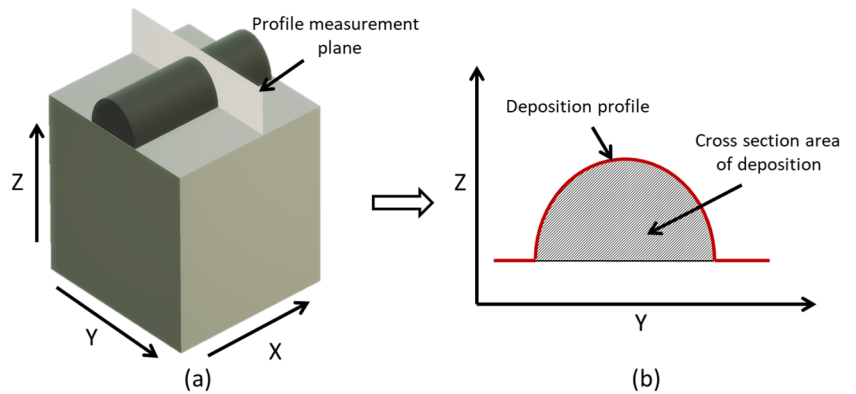
The profiles and the cross-sections of the depositions were evaluated using focus variation microscopy (make: alicona, model: infinite focus) with  $5\times$  magnification. There were 1000 profiles measured per experimental sample, and the average of those profiles was considered for the calculation of the cross-section area. The cross-section area was calculated from profile data using the trapezoidal rule. A schematic of the measurement is shown in Fig. 3.

The mass deposition rates ( $\dot{m}_d$  in g/min) and the powder catchment efficiency (PCE) are determined using the deposition speed (340 mm/min), density ( $7600 \text{ kg/m}^3$ ) and the cross-section area,

**Table 2** Chemical composition of H13 and CPM 9 V

Elements		C	Mn	Si	Cr	Mo	V
CPM 9 V	%	1.9	0.5	0.9	5.2	1.3	9.1
H13	%	0.4	–	–	5.25	1.35	1

**Fig. 3** Schematic of (a) sample with the indication of the plane of measurement, (b) cross section of the deposition



$$PCE = \frac{\dot{m}_d}{\dot{m}_s} \times 100, \tag{1}$$

where  $\dot{m}_d$  is the mass deposition rate and  $\dot{m}_s$  is the powder supply rate (g/min).

### Modeling of the PCE and Clad Shape Evolution

The modeling of the evolution of the deposition shape in DED over an inclined surface is a complex process. Multiple physical phenomena play a role in the final deposition shape. The two key physical aspects are the reduced powder entrapment in the melt pool and the gravity-induced flow of the molten metal due to the angle of inclination. The effect of laser-powder interaction and powder-melt pool interaction to determine the effective melt pool formation have not explicitly been modeled in the CFD model. Instead, a phenomenological model based on experimental data has been used to determine the effective cross-sectional area deposited ( $\frac{\dot{m}}{\rho v}$ ) in CFD. It is only  $\dot{m}$  (mass flow rate) that is determined from the phenomenological model. The methodology adopted for the modeling is shown in Fig. 4.

### Phenomenological modeling of the PCE

For depositions over contoured surfaces, it is very important to study the effect of angle of inclination on the powder catchment efficiency. PCE is a key parameter to assess the process performance as it governs the uniformity of the deposition. Modeling the physics behind the reduction in PCE is

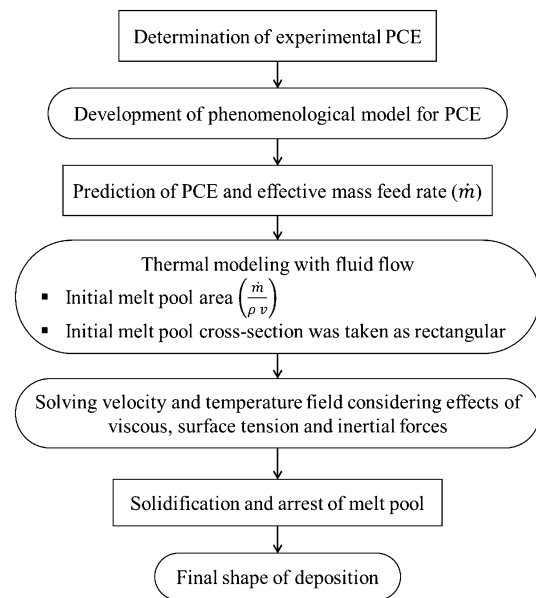


**Fig. 4** Methodology of 2D thermal fluid flow model for shape evolution in DED

challenging, so a phenomenological model is developed to predict the PCE at various angles of inclinations. For this, the depositions carried out in different configurations, i.e., longitudinal, transverse, and oblique, were evaluated for PCE.

The variation of the PCE with the angle of inclination for the longitudinal depositions (case 1) is shown in Fig. 5. Figure 5 shows that the PCE decreases with an increase in the inclination angle for this strategy of deposition.

The PCE is observed to be 65% at an angle of inclination of 0°, i.e. when the substrate surface is horizontal, which

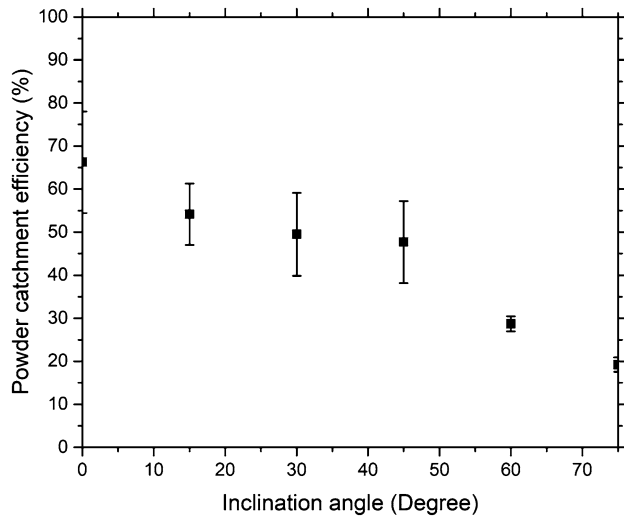


**Fig. 5** Variation of the PCE with the angle of inclination in longitudinal depositions

reduces to 19% if the angle of inclination is increased to 75°. It can be inferred that the loss of powder is significant at higher angles of inclination, which decreases the effective powder entrapment, even though the powder supply rate is quite high. The other thing which can be noted is the sudden decrease in the PCE from 0 to 15°. There is a relatively small decrease in the catchment efficiency between 15 and 45° inclinations, but after that, when the angle of inclination is further increased, the effect becomes much more pronounced. This undesirable loss of powder particles and resulting reduced PCE is a foremost concern for 3D-free form deposition. This reduction in PCE at a higher angle of inclination is because of gravity-induced altered flow dynamics in the nozzle that affects the powder focusing adversely, and the enhanced powder ricochet. The deposition geometry is also expected to be affected due to the reduced PCE at higher angles of inclination.

The second strategy of deposition is transverse depositions (case 2). The variation of the PCE with the angle of inclination for the transverse depositions is shown in Fig. 6. It can be noted that as the angle of inclination increases, the PCE decreases for this deposition strategy as well. The PCE decreases rapidly from 65% at an inclination angle of 0° to 19% at an inclination angle of 15°. When the angle of inclination is increased further, the PCE decreases to a meager 3.5% at an angle of 75°. The gravity-induced powder flow disturbance in the nozzle is exacerbated because the particle trajectories after nozzle exit are disturbed significantly under the effect of gravity. These disturbances deteriorate the powder focusing significantly, and veer the particle away from the melt pool reducing the PCE.

The third strategy of deposition is oblique deposition (case 3). This deposition strategy is a combination of

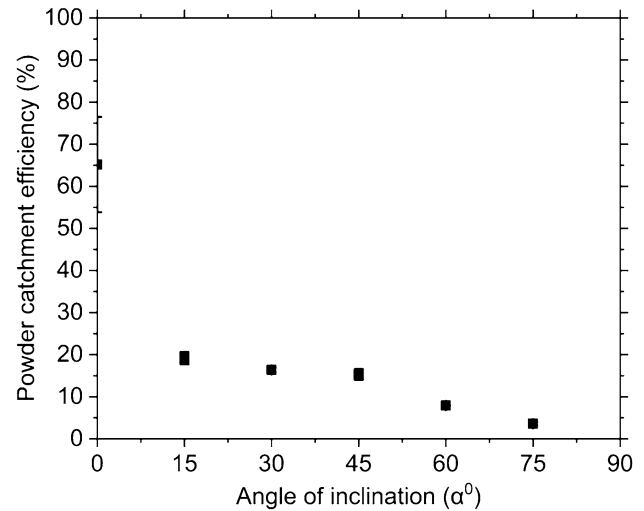


**Fig. 6** Variation of PCE with the angle of inclination for transverse depositions

longitudinal and transverse deposition. The variation of the PCE with the angle of inclination is shown in Fig. 7. If the angle of inclination ( $\beta$ ) is increased from 0 to 15°, there is a steep decrease in the PCE. There is a decrease from 34 to 13.4% in PCE if the angle of inclination is increased from 0 to 15°. As the angle of inclination is increased further above 15°, the PCE nearly remains unchanged between 12 and 15%.

As seen in this section, the powder catchment efficiency is a strong function of the angle of inclination because of the effect of gravity on the powder flow dynamics and the particle trajectories. To keep the laser beam perpendicular to the substrate surface, the direction of the gravity vector

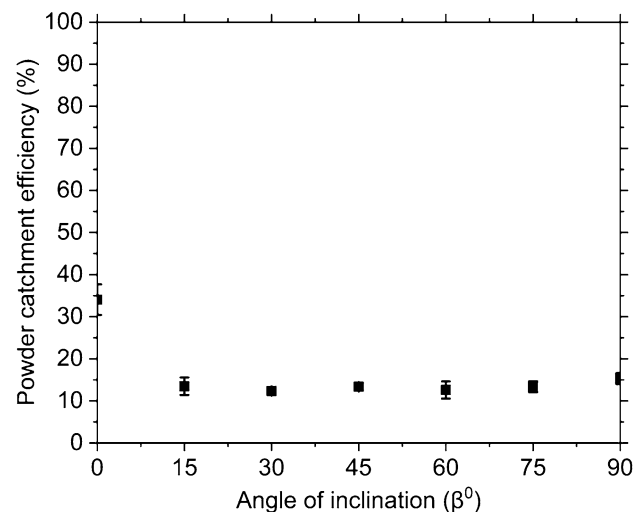


**Fig. 7** Variation of PCE with the angle of inclination for depositions in the oblique direction

changes concerning the deposition head. There is a requirement for a mathematical model to predict the PCE as the gravity vector changes.

The gravity vector has been broken into its three subcomponents, as shown in Fig. 8, to develop a phenomenological model. The first being along the direction of deposition, as represented in Fig. 8b as  $X$ . The second is transverse to the direction of deposition in the plane perpendicular to the substrate surface as shown in Fig. 8b as  $Y$ , and the last one is perpendicular to both the direction of deposition as well as substrate surface as represented in Fig. 8a with  $Z$ . When, there is any change in the angle  $\alpha$  or  $\beta$ , these components of the gravity vector changes. Thus, the powder catchment efficiency can be expressed as a function of these gravity vector components.

It is found that a 4th order polynomial provides good prediction with  $R^2$  value of 99.2%. The obtained empirical model is shown in Eq. (2).

$$\begin{aligned}
 PCE = & -154.43 - 0.0036 g \text{Sin} \alpha \text{Sin} \beta + 0.144 g \text{Sin} \alpha \text{Cos} \beta \\
 & + 4.368 g \text{Cos} \alpha + 1.44 (g \text{Sin} \alpha \text{Sin} \beta)^2 + 1.4(g \text{Sin} \alpha \text{Cos} \beta)^2 \\
 & + 0.0557 (g \text{Sin} \alpha \text{Sin} \beta)^3 + 0.0595 (g \text{Sin} \alpha \text{Cos} \beta)^3 \\
 & + 0.19 (g \text{Cos} \alpha)^3 - 0.0045 (g \text{Sin} \alpha \text{Sin} \beta)^4 \\
 & - 0.0047 (g \text{Sin} \alpha \text{Cos} \beta)^4 - 0.0073 (g \text{Cos} \alpha)^4
 \end{aligned}
 \tag{2}$$

The variation of experimental PCE and the PCE predicted through the developed phenomenological model is shown in Fig. 9a, b.

### Modeling the Shape Evolution

A 2D computational fluid dynamics model is developed to simulate the flow and solidification of the melt pool. The development of this model aims to predict the final deposition geometry in the DED process. The developed model is used to realize the effect of angle of inclination on the deposition shape. As the DED is a complex process, the following assumptions have been made in this model:

**Fig. 8** Schematic for resolving gravity vector into subcomponents

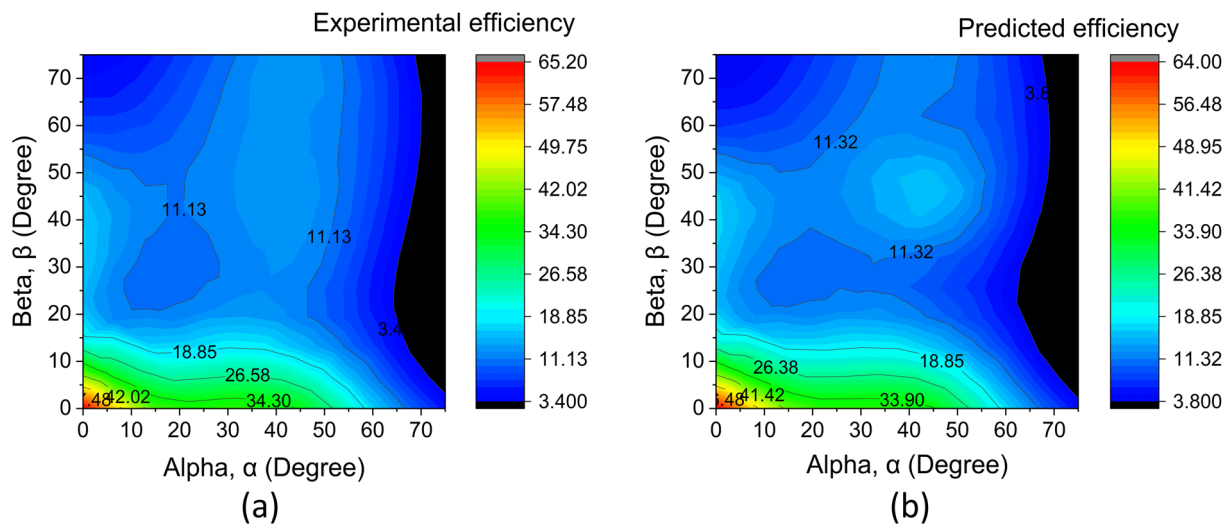
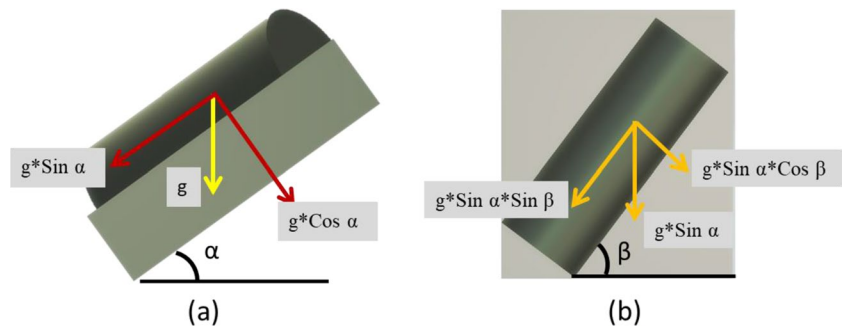


**Fig. 9** Contour plot showing variation of (a) Experimental PCE and (b) Predicted PCE for the combination of  $\alpha, \beta$

- The melting of substrate and powder particles has not been considered in the model. Instead, the shape evolution after melt pool formation is considered in the model.
- The final shape of the deposition cross-section depends upon the melt flow within the plane perpendicular to the deposition direction, and the effect of the melt flow in the direction of deposition is ignored as it will not be significant.
- The effect of the gravity vector along the direction of deposition will not affect the deposition shape significantly, and hence that component of the gravity vector is considered.
- The starting point of the CFD model is a rectangular pool of liquid placed on the substrate.
- The flow of the molten material in the melt pool is assumed to be laminar.

The cross-section area of deposition at various angles of inclination is predicted using the previously developed phenomenological model. The 2D thermal fluid flow model is generated with the predicted melt pool area. After solving for the velocity and temperature field, the melt pool shape is arrested, and the complete melt pool solidifies to provide the deposition shape. The deposition material is modeled as a phase change material.

The Navier Stokes and continuity equations have been solved for the viscous, surface tension, and inertial forces encountered in the melt flow on an inclined substrate. The melt flow due to gravity is primarily responsible for the asymmetric clad cross-sections in depositions on inclined substrates. The continuity and Navier–Stokes equations are given by,

$$\frac{\partial(\alpha_j \rho_j)}{\partial t} + \nabla \cdot (\alpha_j \rho_j v_j) = 0, \quad (3)$$

$$\frac{\partial(\rho v)}{\partial t} + \nabla \cdot (\rho v v) = -\nabla p + \nabla \cdot (\mu \nabla v) + \rho g + S + F, \quad (4)$$

where  $\rho$  is the density,  $p$  is the pressure,  $\mu$  is the viscosity,  $g$  is the gravitational acceleration,  $v$  is the fluid velocity, and  $\alpha_j$  is the volume fraction of  $j^{\text{th}}$  fluid.  $S$  is a source term for solidification, and  $F$  is the source term for surface tension. The free surface of the deposition is tracked using the volume of fluid (VOF) technique using the commercial software ANSYS FLUENT<sup>®</sup>. The total enthalpy content of the melt pool is given by,

$$H = h + \Delta H, \quad (5)$$

$$\text{where } h = h_{\text{ref}} + \int_{T_{\text{ref}}}^T C_p dT,$$

where  $h_{\text{ref}}$  is the reference sensible heat,  $T_{\text{ref}}$  is the reference temperature, and  $C_p$  is the specific heat at constant pressure. The enthalpy porosity technique is used for solidification. In this technique, the liquid–solid front is not tracked explicitly. Instead, liquid fraction is computed at every node using the following equations,

$$\lambda = 0 \text{ if } T \leq T_s, \quad (6)$$

$$\lambda = \frac{T - T_s}{T_l - T_s} \text{ if } T_s < T < T_l, \quad (7)$$

$$\lambda = 1 \text{ if } T > T_l, \quad (8)$$

where  $T_s$  is the solidus temperature and  $T_l$  is the liquidus temperature. Subsequently, the latent heat can be expressed as,

$$\Delta H = \lambda L, \quad (9)$$

where  $L$  is the latent heat of material and  $\Delta H$  can vary between zero for solid and one for liquid. The conduction of the heat from the deposited material to the substrate is solved using the energy equation,

$$\frac{\partial(\rho H)}{\partial t} + \nabla \cdot (\rho v H) = \nabla \cdot (k \nabla T), \quad (10)$$

where  $H$  is the total enthalpy,  $v$  is the velocity, and  $k$  is the thermal conductivity. Now, when  $\lambda$  tends to zero, there will be zero velocity at the node as no liquid fraction, which freezes the melt pool. This is accomplished by the source term  $S$  from Carmon–Kozeney’s equation (Carman 1937) derived from Darcy’s law, which is defined as,

$$S = -\frac{(1 - \lambda)^2}{(\lambda^3 + \varepsilon)} A_{\text{mush}}(v), \quad (11)$$

where  $\varepsilon$  is an infinitesimally small number to prevent the singularity when  $\lambda$  tends to zero.  $A_{\text{mush}}$  is a constant representing the slope for which the melt pool velocity tends to zero when it solidifies.  $A_{\text{mush}} = 10^9$ . The surface tension was modeled using the continuum surface force model present in ANSYS FLUENT. It adds a source term in the momentum equation represented as  $F$  (Brackbill et al. 1992), which is given by,

$$F = \sigma_{ij} \frac{\rho \gamma_i \nabla \alpha_i}{\frac{1}{2}(\rho_i + \rho_j)}, \quad (12)$$



**Table 3** Material property details

Property	Value	Unit
Liquidus temperature	1809	K
Solidus temperature	1776	K
Latent heat of fusion	271,960	J/Kg
Standard state enthalpy	3.29e+08	J/Kg mol
Viscosity	0.0014	Kg/m s
Thermal conductivity	43	W/m K
Specific heat	658	J/kg K
Density	7750	Kg/m <sup>3</sup>
Surface tension coefficient	0.4	N/m

where  $\sigma$  is the surface tension coefficient,  $\alpha$  is the volume fraction, and  $\gamma$  is the curvature of the interface. The  $i$  and  $j$  are fluids. The thermo-physical properties used for the simulations are listed in Table 3.

## Results and Discussion

### Comparison of the Predicted and Experimental Deposition Profiles

The simulations were performed for every experimental condition. This section focuses on the comparison of the simulated deposition profile with the experimentally obtained profile. The initial cross-sectional area of deposit in the CFD model has been taken from the phenomenological model developed based on experimental data. The evolved shape from the CFD model in terms of heights, widths, and actual deposition profiles have been compared with the experimental results.

#### Longitudinal Deposition

In the case of longitudinal deposition, the component of the gravity vector along the direction of deposition is zero. There will only be two components of the gravity, namely the sideward component ( $g \sin \alpha$ ) and downward component (normal to the substrate surface),  $g \cos \alpha$  (see Fig. 8). Where the downward component forces the pool to stay adhered to the substrate and the sideward component gives the melt pool a sideward flow resulting in asymmetry in the deposition profile. Figure 10 shows the predicted and experimental heights and widths for various angles of inclination.

It can be observed that the height of the deposition decreases significantly as the angle of inclination is increased. There is a decrease of  $\sim 82\%$  in the deposition height and  $\sim 9\%$  in deposition width if the angle of inclination is increased from 0 to 75°. The model predicts the

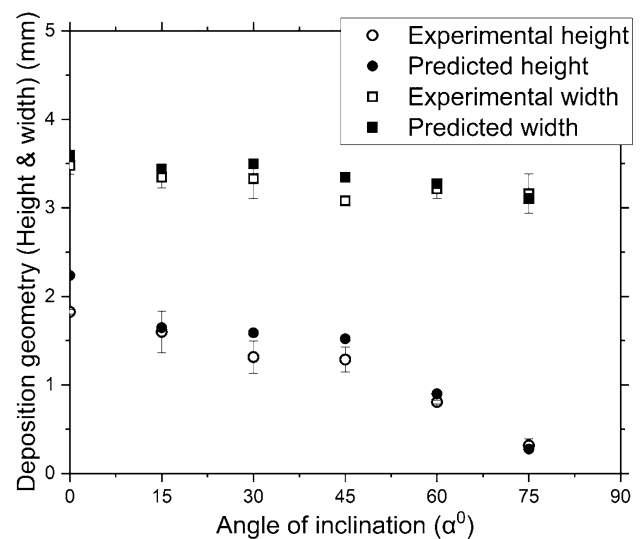


**Fig. 10** Predicted and experimental height and width for longitudinal deposition

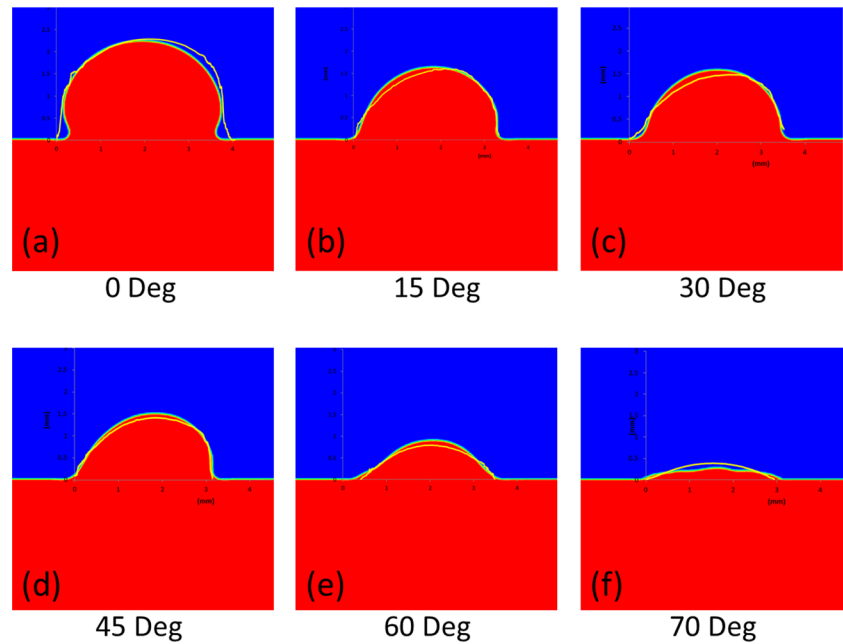
height and width quite well, as seen in Fig. 10. The prediction errors for height and lie within 22.4% and 8.7%, respectively.

Figure 11 shows the comparison of the experimental and simulated deposition profiles. The red color is the simulated profile, whereas the yellow profile is measured from the experimental deposition. It can be seen from Fig. 11 that the simulated profiles are in a good match with the experimental ones. This further corroborates that the model is effectively capturing the gravity-driven melt flow before solidification. The small deviation present at a higher angle of inclination is due to an error in the prediction of powder catchment efficiency.

#### Transverse Deposition

In the transverse depositions, there will not be any component of gravity pushing the melt pool sideward, i.e., the sideward component of gravity will be zero. This ensures symmetry in the deposition profiles. The variation of predicted and experimental height and width of the deposition is shown in Fig. 12. In this case, as well the decrease in the height is very significant, whereas the variation in width is insignificant. There is a decrease of  $\sim 88\%$  in height as the angle of inclination is increased from 0 to 75°. The width seems to be increasing as the angle of inclination is increased. This can be attributed to the fact that there will be a flow of molten metal in line with the direction of deposition. This trend in the predicted widths is not similar as the gravity component responsible for this was neglected in 2D

**Fig. 11** Actual and predicted deposition profiles at inclinations of (a) 0°, (b) 15°, (c) 30°, (d) 45°, (e) 60°, and (f) 75° with depositions performed parallel to pivot line



CFD simulation. Hence, the maximum prediction error in height and width is 24% and 11.5%, respectively. The comparison of simulated and experimental deposition profiles is shown in Fig. 13. It can be observed from Fig. 13 that the simulated profiles match well with the experimentally measured profiles. At an angle of inclination of 45°, the simulated deposition over predicting a little bit. This is again due to the prediction errors in the PCE.

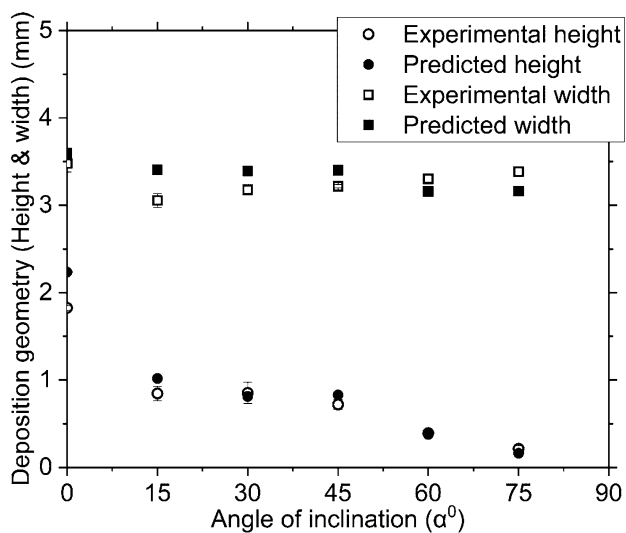


**Fig. 12** Predicted and experimental height and width for transverse deposition

### Oblique Deposition

The oblique strategy of deposition is a combination of both angles  $\alpha$  and  $\beta$ . All three components of gravity, i.e.,  $g \sin \alpha \sin \beta$ ,  $g \sin \alpha \cos \beta$  and  $g \cos \alpha$  act together on the melt pool. The component  $g \cos \alpha$  acting normal to the substrate surface is constant as the angle  $\alpha$  is kept constant at 45°. However, the other components vary with variation in angle  $\beta$  the component  $g \sin \alpha \sin \beta$  is neglected in the 2D CFD simulation. The variation of predicted and experimental height and width is shown in Fig. 14. The variation in the height and the width of deposition with the angle of inclination, in this case, is not very significant. The height and width remain constant with the angle of inclination. The prediction errors for width and height lie within 6.8% and 24%, respectively, except at an inclination angle of 45°. At 45°, the prediction error in PCE from the phenomenological model is slightly high, which leads to a large deviation in the predicted height.

The comparison of the simulated and experimental profiles for oblique deposition is shown in Fig. 15. It can be seen that the empirical model for PCE is good enough, but profiles are slightly over and under predicting at some points.

### Process Recommendations

It is important to note that for all strategies of depositions, the PCE is very significantly affected by the angle of inclination. As the inclination is increased from 0°, the PCE is observed to have a substantial drop. This setup is not a viable option for depositions over higher angles of inclination. However, one can go up to 45° inclination, but if the

**Fig. 13** Actual and predicted deposition profiles at inclinations of (a) 0°, (b) 15°, (c) 30°, (d) 45°, and (e) 60° with depositions perpendicular to pivot line

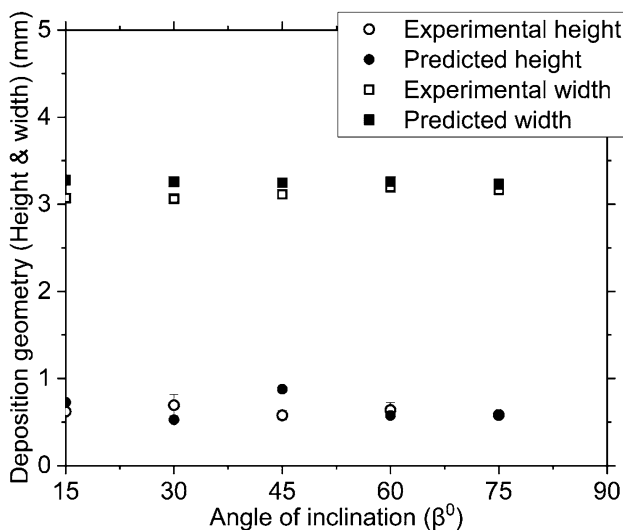
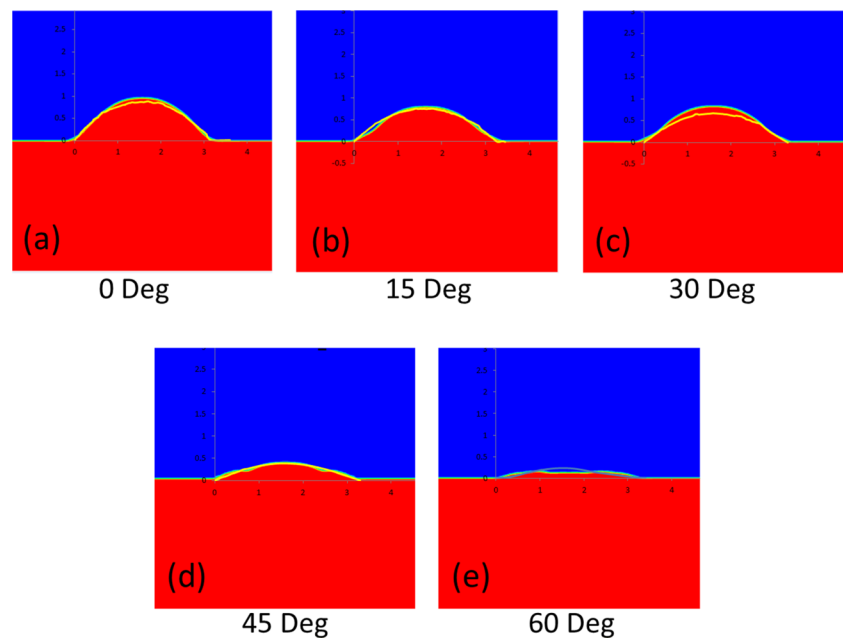


**Fig. 14** Predicted and experimental height and width for oblique deposition

inclination is increased further, the deterioration of PCE becomes much severe. So, it is being recommended that the inclination angle should be kept below 45°.

The transverse deposition results in a symmetric clad profile as there is no gravity vector acting on the melt pool to force the molten metal flow sideward. However, the longitudinal depositions are prone to asymmetry due to the sideward gravity vector. One should not worry about this asymmetry, where multiple side-by-side layers need to be

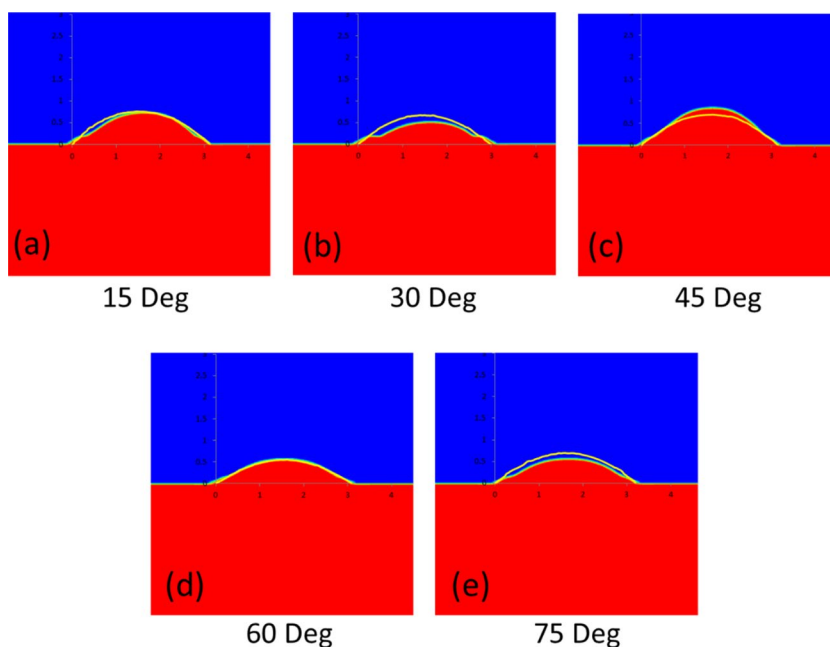
deposited, as the material starved side of the deposition will be covered by another track. The oblique deposition is observed to consistent for PCE, but the efficiencies are quite low, so it cannot be recommended.

## Conclusions

In this paper, the effect of angle of inclination on the powder catchment efficiency and the clad shape evolution has been studied. In addition to the experimental characterization, the clad shape evolution as a function of inclination angle has been modeled via CFD. The following conclusions can be drawn from this paper:

- The powder catchment efficiency is a very strong function of the angle of inclination. Under the experimental conditions investigated, the PCE has fallen below 5% at an angle of inclination of 75°.
- There are two major factors contributing to the evolution of deposition shape, namely, the power loss due to gravity-induced powder flow dynamics in the nozzle and beyond with the angle of inclination and gravity-driven melt flow.
- The 2D CFD model has been developed incorporating the effects of the melt-flow and solidification.
- The model captures the effect of angle of inclination in terms of reduction in PCE and the gravity-driven melt flow effectively. The simulated deposition profiles are in good match with the experimentally obtained profiles.

**Fig. 15** Actual and predicted deposition profiles at inclinations of (a) 15°, (b) 30°, (c) 45°, (d) 60°, and (e) 75° in oblique depositions strategy



**Acknowledgements** The authors wish to gratefully acknowledge that this research was funded by the DST-Swarnajayanti Fellowship award [DST/SJF/ETA-02/2014-2015] and Technology Systems Development Program [DST/TSG/AMT/2015/226/G], Government of India.

**Funding** This work was funded by the DST-Swarnajayanti Fellowship award [DST/SJF/ETA-02/2014-2015] and the Technology Systems Development Program [DST/TSG/AMT/2015/226/G], Government of India.

**Data availability** The data generated during this work is available from the corresponding author upon reasonable request.

**Code availability** Available upon request to the corresponding author.

## Declarations

**Competing interests** The authors declare no competing interests.

## References

- Alya S, Keshav K, Singh R (2017) Characterization of clad geometry and bond strength in micro-scale laser cladding of steels. In: Liao Y-S, Shih AJ, Lin C-F (eds) World congress on micro and nano manufacturing (WCMNM). Kaohsiung, Taiwan, pp 21–24
- Alya S, Singh R (2021) Discrete phase modeling of the powder flow dynamics and the catchment efficiency in laser directed energy deposition with inclined coaxial nozzles. *J Manuf Sci Eng*. <https://doi.org/10.1115/1.4049966>
- Alya S, Vundru C, Ankamreddy B, Singh R (2019) Characterization and modeling of deposition geometry in directed energy deposition over inclined surfaces. *Procedia Manuf* 34:695–703. <https://doi.org/10.1016/j.promfg.2019.06.225>
- Alya S, Vundru C, Ankamreddy B et al (2021) Development and modeling of a robotic restoration system based on laser directed energy deposition. *Trans Indian Inst Met*. <https://doi.org/10.1007/s12666-020-02151-z>
- Brackbill JU, Kothe DB, Zemach C (1992) A continuum method for modeling surface tension. *J Comput Phys* 100:335–354. [https://doi.org/10.1016/0021-9991\(92\)90240-Y](https://doi.org/10.1016/0021-9991(92)90240-Y)
- Bruck G, Shinn B, Kamel A (2012) A study of the effect of angle of beam incidence on ytterbium fiber laser cladding of alloy 625. *Int Congr Appl Lasers Electro-Optics* 156:156–165. <https://doi.org/10.2351/1.5062437>
- Carman PG (1937) Fluid flow through granular beds. *Chem Eng Res Des* 15:S32–S48. [https://doi.org/10.1016/s0263-8762\(97\)80003-2](https://doi.org/10.1016/s0263-8762(97)80003-2)
- Fallah V, Alimardani M, Corbin SF, Khajepour A (2011) Temporal development of melt-pool morphology and clad geometry in laser powder deposition. *Comput Mater Sci* 50:2124–2134. <https://doi.org/10.1016/j.commatsci.2011.02.018>
- Hao J, Meng Q, Li C et al (2019) Effects of tilt angle between laser nozzle and substrate on bead morphology in multi-axis laser cladding. *J Manuf Process* 43:311–322. <https://doi.org/10.1016/j.jmapro.2019.04.025>
- Hu YP, Chen CW, Mukherjee K (1998) Development of a new laser cladding process for manufacturing cutting and stamping dies. *J Mater Sci* 33:1287–1292. <https://doi.org/10.1023/A:1004346214050>
- Jhavar S, Paul CP, Jain NK (2013) Causes of failure and repairing options for dies and molds: a review. *Eng Fail Anal* 34:519–535. <https://doi.org/10.1016/j.engfailanal.2013.09.006>
- Kattire P, Paul S, Singh R, Yan W (2015) Experimental characterization of laser cladding of CPM 9V on H13 tool steel for die repair applications. *J Manuf Process* 20:492–499. <https://doi.org/10.1016/j.jmapro.2015.06.018>
- Lalas C, Tsiaras K, Salonitis K, Chryssolouris G (2007) An analytical model of the laser clad geometry. *Int J Adv Manuf Technol* 32:34–41. <https://doi.org/10.1007/s00170-005-0318-0>
- Leunda J, Soriano C, Sanz C, Navas VG (2011) Laser cladding of vanadium-carbide tool steels for die repair. *Phys Procedia* 12:345–352. <https://doi.org/10.1016/J.PHPRO.2011.03.044>
- Lin J, Hwang B-C (1999) Coaxial laser cladding on an inclined substrate. *Opt Laser Technol* 31:571–578. [https://doi.org/10.1016/S0030-3992\(99\)00116-4](https://doi.org/10.1016/S0030-3992(99)00116-4)

- Paul CP, Mishra SK, Kumar A, Kukreja LM (2013) Laser rapid manufacturing on vertical surfaces: analytical and experimental studies. *Surf Coatings Technol* 224:18–28. <https://doi.org/10.1016/j.surfcoat.2013.02.044>
- Paul S, Singh R, Yan W (2016) Thermal model for additive restoration of mold steels using crucible steel. *J Manuf Process* 24:346–354. <https://doi.org/10.1016/j.jmapro.2016.06.012>
- Paul S, Thool K, Singh R et al (2017) Experimental characterization of clad microstructure and its correlation with residual stresses. *Procedia Manuf* 10:804–818. <https://doi.org/10.1016/j.promfg.2017.07.081>
- Qi H, Mazumder J, Ki H (2006) Numerical simulation of heat transfer and fluid flow in coaxial laser cladding process for direct metal deposition. *J Appl Phys*. <https://doi.org/10.1063/1.2209807>
- Vundru C, Singh R, Yan W, Karagadde S (2019) Non-dimensional process maps for normalized dilution limits in laser direct metal deposition. *Procedia manuf* 34:712–721. <https://doi.org/10.1016/j.promfg.2019.06.227>
- Vundru C, Singh R, Yan W, Karagadde S (2020a) The effect of martensitic transformation on the evolution of residual stresses and identification of the critical linear mass density in direct laser metal deposition-based repair. *J Manuf Sci Eng Trans ASME* 142:1–13. <https://doi.org/10.1115/1.4046828>
- Vundru C, Singh R, Yan W, Karagadde S (2020) Non-dimensional process maps for residual stress in laser directed energy deposition. *Procedia manuf* 48:697–705. <https://doi.org/10.1016/j.promfg.2020.05.102>
- Wang S-H, Chen J-Y, Xue L (2006) A study of the abrasive wear behaviour of laser-clad tool steel coatings. *Surf Coatings Technol* 200:3446–3458. <https://doi.org/10.1016/J.SURFCOAT.2004.10.125>
- Xue L, Chen J, Wang SH (2013) Freeform laser consolidated H13 and CPM 9V tool steels. *Metallogr Microstruct Anal* 2:67–78. <https://doi.org/10.1007/s13632-013-0061-0>
- Zhu G, Shi S, Fu G et al (2017) The influence of the substrate-inclined angle on the section size of laser cladding layers based on robot with the inside-beam powder feeding. *Int J Adv Manuf Technol* 88:2163–2168. <https://doi.org/10.1007/s00170-016-8950-4>

**Publisher's Note** Springer Nature remains neutral with regard to jurisdictional claims in published maps and institutional affiliations.